Supplementary Information

Sensing of ultra-ppm level NO_2 gas via synergistic effects of Cr Doping and E-Beam Irradiation in WO_3 nanostructures

Anusha[1], Poornesh P[1*], Vikash Chandra Petwal[2], Vijay Pal Verma[2], Jishnu Dwivedi[2]

[1]Department of Physics, Manipal Institute of Technology, Manipal Academy of Higher Education, Manipal, Karnataka, 576104, INDIA

[2]Industrial Accelerator Section, PSIAD, Raja Ramanna Centre for Advanced Technology, Indore 452012, M.P., INDIA

* Corresponding author.

Email addresses: poornesh.p@manipal.edu, poorneshp@gmail.com *(Poornesh P)*

S1. Structural insights from XRD

Various structural parameters, including crystallite size, strain, and dislocation density, were calculated using the eqns. (S1)-(S3). Scherrer's equation [1] was utilized to determine the crystallite size (D), expressed as follows:

$$D = \frac{0.9\,\lambda}{\beta cos\theta} \qquad (S1)$$

β denotes full-width half maximum (FWHM), θ is angle between the incident X-ray and the crystal plane, and λ is given as 0.154 nm for Cu-Kα source.

Dislocation density (δ) and strain (ε) [2,3] was computed using the following formulae,

$$\delta = \frac{1}{D^2} \qquad (S2)$$

$$\varepsilon = \frac{\beta}{4\,tan\theta} \qquad (S3)$$

S2. Bandgap studies

Absorbance studies of the Samples A, B and C were performed using UV-Visible spectrophotometer. Fig. S1(a & b) indicates the absorbance spectra in the visible region and

corresponding Tauc's plot. Band gap values of the films were evaluated via Tauc's relation, wherein $(\alpha h\nu)^2$ is plotted against incident photon energy [4]. Energy band gaps were estimated as 3.22 eV, 3.10 eV and 3.13 eV for WO_3 (Sample A), Cr-WO_3 (Sample B), and EBI Cr-WO_3 (Sample C), films, respectively.

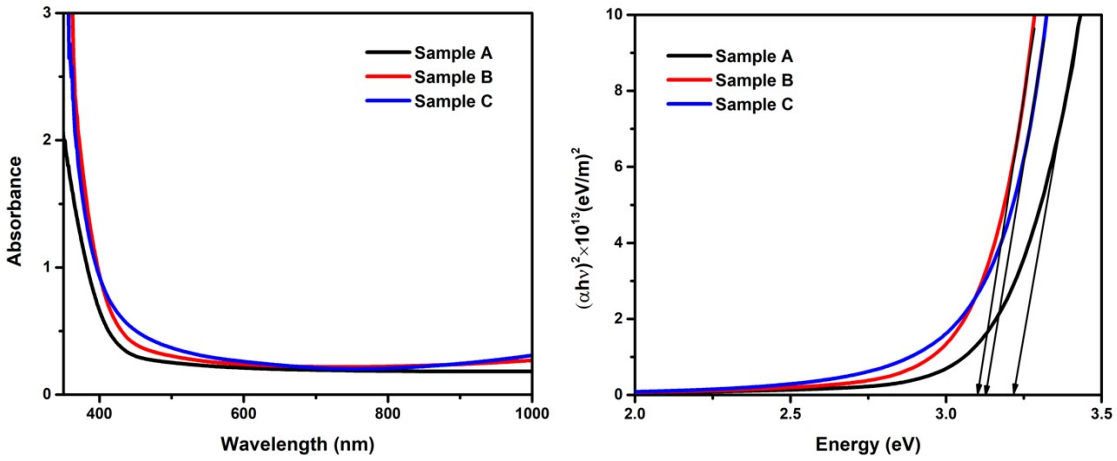

Fig. S1. (a) Absorbance spectra (b) Tauc's plot of Samples A, B and C.

S3. NO_2 sensing measurements

The theoretical limit of detection (LOD) for the EBI Cr-WO_3 sensor was calculated by plotting the sensor response against various NO_2 concentrations using linear regression (y = a + bx) and applying eqn. (S4) [5].

$$LOD = 3\sigma_D/s \qquad (S4)$$

Where, σ_D is the standard deviation of the y-intercept and s is the slope of the calibration curve. The results indicated that the theoretical limit of detection for the EBI Cr-WO_3 (Sample C) sensor was 0.4 ppm.

Table S1. Comparison of NO_2 sensing data with literature.

Material	**Method**	**Gas Conc. (ppm)**	**Operating Temperature (°C)**	**Sensor Response**	**Reference**
In_2O_3 decorated WO_3	Hydrothermal & Thermal evaporation	200	300	28	[6]
Mesoporous WO_3	One-step precipitation	200	250	99.78	[7]
Ag doped WO_3	Soft chemical route	100	200	1.5	[8]
WO_3 nanoflowers	Hydrothermal	100	200	2.25	[9]
Annealed + Laser irradiated WO_3	RF Sputtering	0.5	200	6.7	[10]
EB irradiated Pd-rGO	Solution processing & Thermal annealing	10	RT	1.05	[11]
EB irradiated Cr-WO_3	Spray pyrolysis	5	200	3.43	Present work

References

[1] Scherrer P. Bestimmung der Grösse und der inneren Struktur von Kolloidteilchen mittels Röntgensrahlen"[Determination of the size and internal structure of colloidal particles using X-rays]. Nachr Ges Wiss Goettingen, Math-Phys Kl 1918;26:98–100.

[2] Bindu P, Thomas S. Estimation of lattice strain in ZnO nanoparticles: X-ray peak profile analysis. Journal of Theoretical and Applied Physics 2014;8:123–34.

[3] Kumar N, Sidhu GK, Kumar R. Correlation of synthesis parameters to the phase segregation and lattice strain in tungsten oxide nanoparticles. Mater Res Express 2019;6. https://doi.org/10.1088/2053-1591/ab12a5.

[4] Makuła P, Pacia M, Macyk W. How To Correctly Determine the Band Gap Energy of Modified Semiconductor Photocatalysts Based on UV-Vis Spectra. Journal of Physical Chemistry Letters 2018;9:6814–7. https://doi.org/10.1021/acs.jpclett.8b02892.

[5] Liu H, Shen W, Chen X. A room temperature operated ammonia gas sensor based on Ag-decorated TiO_2 quantum dot clusters. RSC Adv 2019;9:24519–26. https://doi.org/10.1039/c9ra05439a.

[6] Nam B, Ko T-K, Hyun S-K, Lee C. NO_2 sensing properties of WO_3-decorated In_2O_3 nanorods and In_2O_3-decorated WO_3 nanorods. Nano Converg 2019;6:40. https://doi.org/10.1186/s40580-019-0205-2.

[7] Zhang C, Hong X, Jiang C, Luo F, Wan B, Zheng X. A special gas sensor based on mesoporous WO_3 sensing electrode in medium low temperature for NO_2 detection. Mater Lett 2022;306:130927. https://doi.org/10.1016/j.matlet.2021.130927.

[8] Pandey NK, Roy A, Tiwari K, Mishra A, Rai A, Jayaswal S, Rashmi, Madhvendra, Govindan A. NO_2 sensing studies of WO_3 and Ag doped WO_3 prepared through sol-gel route. 2012 1st International Symposium on Physics and Technology of Sensors (ISPTS-1), 2012, p. 342–5. https://doi.org/10.1109/ISPTS.2012.6260963.

[9] Hingangavkar GM, Navale YH, Nimbalkar TM, Mulik RN, Patil VB. Hydrothermally engineered WO3 nanoflowers: A selective detection towards toxic NO_2 gas. Sens Actuators B Chem 2022;371:132584. https://doi.org/10.1016/j.snb.2022.132584.

[10] Zhang C, Van Overschelde O, Boudiba A, Snyders R, Olivier M-G, Debliquy M. Improvement of sensing characteristics of radio-frequency sputtered tungsten oxide films through surface modification by laser irradiation. Mater Chem Phys 2012;133:588–91. https://doi.org/10.1016/j.matchemphys.2012.01.116.

[11] Choi MS, Mirzaei A, Bang JH, Oum W, Kim SS, Kim HW. Improvement of NO_2 Sensing Properties in Pd Functionalized Reduced Graphene Oxides by Electron-Beam Irradiation. Front Mater 2019;6:197. https://doi.org/10.3389/fmats.2019.00197.